Available online at www.sciencedirect.com
ScienceDirect
International Journal of Heat and Mass Transfer 50 (2007) 977–990
International Journal of HEAT and MASS TRANSFER
www.elsevier.com/locate/ijhmt

Steady forced convection heat transfer from a heated circular cylinder to power-law fluids

Ram Prakash Bharti [a], R.P. Chhabra [a,*], V. Eswaran [b]

[a] Department of Chemical Engineering, Indian Institute of Technology, Kanpur 208016, India
[b] Department of Mechanical Engineering, Indian Institute of Technology, Kanpur 208016, India

Received 12 January 2006
Available online 12 October 2006

Abstract

Forced convection heat transfer to incompressible power-law fluids from a heated circular cylinder in the steady cross-flow regime has been investigated numerically by solving the momentum and thermal energy equations using a finite volume method and the QUICK scheme on a non-uniform Cartesian grid. The dependence of the average Nusselt number on the Reynolds number ($5 \leqslant Re \leqslant 40$), power-law index ($0.6 \leqslant n \leqslant 2$) and Prandtl number ($1 \leqslant Pr \leqslant 1000$) has been studied in detail. The numerical results are used to develop simple correlations as functions of the pertinent dimensionless variables. In addition to the average Nusselt number, the effects of Re, Pr and n on the local Nusselt number distribution have also been studied to provide further physical insights. The role of the two types of thermal boundary conditions, namely, constant temperature and uniform heat flux on the surface of the cylinder has also been presented.
© 2006 Elsevier Ltd. All rights reserved.

Keywords: Steady flow; Power-law fluids; Shear-thinning; Shear-thickening; Circular cylinder; Nusselt number; Constant wall temperature; Uniform heat flux

1. Introduction

The steady cross-flow past a circular cylinder represents an idealization of many industrially important processes. Typical examples include the flow on the shell side of tubular heat exchangers, pin fins, the use of thin wires as measuring sensors and probes, the use of screens to filter polymer melts and sewage sludges, etc. In addition to such an overwhelming pragmatic significance, this flow is also regarded to be one of the classical problems of fluid mechanics. Consequently, a voluminous body of information on a variety of flow phenomena associated with this configuration has accumulated over the years, albeit most of it relates to the Newtonian fluids. Several excellent survey articles and books summarizing the current state of the art for Newtonian fluid flow past a circular cylinder are now available [1–11]. Hence, adequate information is now available on most aspects of flow and heat transfer for Newtonian fluid flow past a circular cylinder. Suffice it to say here that even for Newtonian fluids, the flow characteristics have been studied much more extensively than the corresponding heat or mass transfer problems.

On the other hand, many materials of industrial significance exhibit a range of non-Newtonian fluid behaviour features. For instance, most polymeric systems (melts and solutions) and slurries exhibit shear dependent viscosity thereby displaying shear-thinning or shear-thickening, or both, under appropriate conditions. Despite their wide occurrence in fiber reinforced resin processing, in the handling of paper pulp suspensions, fluidization of fibrous materials, etc., very little work is currently available on the cross-flow of shear-thinning and shear-thickening fluids which are frequently modelled by the simple power-law model [12,13] over a circular cylinder. The available literature for the flow past a single cylinder and across a periodic array of cylinders [2,14,15] seems to suggest the viscoelastic effects to be minor in this flow configuration. Furthermore,

* Corresponding author. Tel.: +91 512 2597393; fax: +91 512 2590104.
E-mail address: chhabra@iitk.ac.in (R.P. Chhabra).

0017-9310/$ - see front matter © 2006 Elsevier Ltd. All rights reserved.
doi:10.1016/j.ijheatmasstransfer.2006.08.008

Nomenclature

c_p	specific heat of the fluid (J/kg K)
CWT	constant wall temperature
D	diameter of the cylinder (m)
FVM	finite volume method
h	local convective heat transfer coefficient (W/m^2 K)
I_2	second invariant of the rate of the strain tensor (–)
j	Colburn factor for heat transfer (–)
k	thermal conductivity of the fluid (W/m K)
L_d	downstream length from the center of the cylinder to outlet (–)
L_u	upstream length from the inlet to the center of the cylinder (–)
L_x	length of the domain (–)
L_y	half height of the domain (–)
m	power-law consistency index (Pa s^n)
n	power-law behaviour index (–)
n_s	direction normal to the cylinder surface (–)
Nu	average Nusselt number (–)
$Nu(0)$	Nusselt number at the front stagnation ($\theta = 0$) point (–)
$Nu(\theta)$	local Nusselt number (–)
$Nu(\pi)$	Nusselt number at the rear stagnation ($\theta = \pi$) point (–)
p	pressure (–)
p_∞	pressure at the exit (–)
Pe	Peclet number (–)
Pr	Prandtl number (–)
q_w	heat flux on the surface of the cylinder (W/m^2)
QUICK	quadratic upwind interpolation for convective kinematics
Re	Reynolds number (–)
t	time (–)
T	temperature (–)
T_w	temperature at the surface of the cylinder (K)
T_∞	temperature of the fluid at the inlet (K)
U_∞	uniform velocity of the fluid at the inlet (m/s)
UHF	uniform heat flux
V_x, V_y	x- and y-components of velocity (–)
x	streamwise coordinate (–)
y	transverse coordinate (–)

Greek symbols

ϵ_{ij}	component of the rate of the strain tensor (–)
η	viscosity (–)
θ	angular displacement from the front stagnation point (degree)
ρ	density of the fluid (kg/m^3)
τ_{ij}	shear stress (–)

the fluid relaxation time often shows a dependence on the shear rate, which is similar to shear-dependence of viscosity. Thus, the relaxation time will also decrease with the increasing value of the Reynolds number thereby a suitably defined Deborah number would also be small. On this count, the viscoelastic effects are not expected to be significant in this case. Therefore, it seems to be reasonable to begin with the flow of purely viscous power-law type fluids as long as the power-law constants are evaluated in the shear rate range appropriate for the flow over a cylinder and the level of complexity can gradually be built up to accommodate other non-Newtonian characteristics. This work is thus concerned with the convective heat transfer from a heated circular cylinder to streaming power-law fluids. It is useful to briefly review the prior scant available literature before presenting the new results obtained in this study.

2. Previous work

It is well known that the so-called Stokes paradox is irrelevant for shear-thinning fluids, as the viscous forces dominate the flow even faraway from the cylinder [16,17]. Consequently, reliable results on the drag of a cylinder in power-law fluids (shear-thinning fluids) are now available in the so-called creeping (zero Reynolds number) flow regime [16,18,19]; these results are in excellent agreement with each other. These low Reynolds number results have been complemented by 2-D numerical simulations up to Reynolds number values of 40 for a range of values of the power-law index [20–24]. Combined together, reliable values of the individual and total drag coefficients for the 2-D steady cross-flow of power-law fluids past a circular cylinder are now available up to $Re \leqslant 40$ and for $0.5 \leqslant n \leqslant 2$. In addition to the macroscopic flow parameters like drag, Bharti et al. [23] also reported extensive results on the detailed streamline contours, surface pressure, vorticity and viscosity for a range of conditions, thereby elucidating the complex role of power-law rheology in this flow configuration. Recently, Sivakumar et al. [25] reported the critical values of the Reynolds number marking the end of creeping and that of steady symmetric flow regime for the cross-flow of a power-law fluids ($0.3 \leqslant n \leqslant 1.8$) past a circular cylinder. The analogous problem of axial flow of Carreau model fluids along the axis of a cylinder has recently been investigated by Hsu et al. [26].

On the other hand, as far as known to us, there has been only one study on forced convection heat transfer to power-law fluids from a heated cylinder. Soares et al. [22] used the stream function-vorticity approach to solve the momentum and thermal energy equations to obtain the

detailed velocity and temperature fields for three values of Reynolds number (5, 20 and 40) as functions of the power-law index and Prandtl number (1–100). They approximated the unconfined flow condition by enclosing the cylinder in a cylindrical envelope of fluid of diameter ranging from 12.2 to 54.6 times that of the radius of the cylinder. Therefore, their results could have been influenced by the wall effects. Furthermore, they solved the momentum and energy equations in cylindrical coordinates with an exponential transformation in the radial direction. Aside from these results based on the solution of the complete governing equations, there have been some heat transfer studies based on the boundary layer flow approximations, e.g. see [27–31, etc.] and most of these have been reviewed elsewhere [2,4].

There have been a very few experimental studies of this problem and most of these relate to the higher Reynolds and/or Prandtl number conditions [32–37]. In the only studies on heat transfer from heated cylinders to power-law fluids, Mizushina et al. [33] and Takahashi et al. [32] reported mean Nusselt number over the following ranges of conditions: $0.72 \leqslant n \leqslant 1.0$; $43 \leqslant Re \leqslant 19{,}200$ and $5.6 \leqslant Pr_m \leqslant 40{,}000$; and $0.784 \leqslant n \leqslant 1.0$ and $40 \leqslant Re \leqslant 4000$, respectively. These heat transfer results have been supplemented by limited mass transfer results from short cylinders in the range as $0.5 \leqslant L/D \leqslant 1.8505$, $0.751 \leqslant n \leqslant 1.0$; $0.0118 \leqslant Re \leqslant 2500$ and $856 \leqslant Pr_m \leqslant 5.95 \times 10^5$ by Kumar et al. [34], $0.89 \leqslant n \leqslant 1.0$ and $0.0018 \leqslant Re \leqslant 513$ by Ghosh et al. [35]. In all such experimental studies, empirical correlations have been presented which are evidently restricted to the rather narrow range of experimental conditions. Furthermore, none of these have been validated using independent experimental data. More recently, vortex shedding characteristics from a circular cylinder in power-law fluids have been studied by Coelho et al. [38] and Coelho and Pinho [39,40] in the range of Reynolds number of 50–9000, and power-law indices of 0.543–0.880 for power-law fluids and 0.5127–0.6311 for Carreau–Yasuda fluids, for 5 and 10% blockage (H/D) and of aspect (L/D) ratios of 12 and 6. The main findings of these works [38–40] were that: (a) an increase in either the shear-thinning tendency, aspect ratio and fluid elasticity reduce the various critical Reynolds numbers marking the end of the various flow regimes, (b) the fluid elasticity reduces the extension of the transition regime and increases the formation length (which decreases the Strouhal number in the laminar shedding regime) and (c) the cylinder boundary layer thickness increases and therefore the diffusion length reduces (which increases the Strouhal number) with an increase in the shear-thinning tendency. Ogawa et al. [41] experimentally investigated the viscoelastic effects on the forced convection mass transfer in polymer solutions around a sphere and a circular cylinder in the Reynolds number range $1 \leqslant Re \leqslant 200$. Similarly, there have been a few studies on the sedimentation of cylinders in power-law fluids [42,43], but the main thrust of these studies was to develop drag correlations. Finally, there have been a few numerical studies on the forced convection heat transfer to power-law fluids from a square cylinder [44,45], from a sphere [46] and from tube banks [47].

Thus, very little reliable information is available on the two-dimensional steady forced convection heat transfer in power-law fluids from a circular cylinder at moderate values of the Reynolds and Prandtl numbers. This paper aims to fill this gap in the literature. In particular, the thermal energy equation has been solved numerically for a range of values of the Reynolds and Prandtl numbers and power-law index using a finite volume method to obtain the detailed temperature field around the cylinder, which in turn are used to deduce the local and average values of the heat transfer coefficient. The Reynolds number was systematically incremented in steps of 5 in the range 5–40, Prandtl number varied in the range 1–1000 and power-law index in the range $0.6 \leqslant n \leqslant 2$, thereby embracing both shear-thinning and shear-thickening fluid behaviour. In addition, the role of the two limiting cases of the thermal boundary condition, namely, constant temperature and constant heat flux on the surface of the cylinder has been investigated. The paper is concluded by presenting a preliminary comparison with the prior results available in the literature.

3. Problem statement and mathematical formulation

Consider the 2-D cross-flow of uniform velocity U_∞ and temperature T_∞ past a long circular cylinder of diameter D. The unconfined flow is simulated here by considering the flow in a channel with the cylinder placed symmetrically between the two plane walls with slip boundary conditions (Fig. 1), as opposed to the concentric cylindrical domain used by Soares et al. [22].

While in practice, the thermal boundary conditions on the surface of the cylinder can be quite involved, it is customary to consider the two limiting conditions, namely, either the constant temperature (CWT), T_w, or at a uniform heat flux (UHF), q_w imposed on the surface of the cylinder. Furthermore, the thermo-physical properties of the fluids (ρ, m, n, c_p and k) are assumed to be independent of temperature and that the viscous dissipation is negligible. While this approximation is reasonable for each of the relevant physical properties, except for the power-law index (n) and power-law consistency index (m). Thus, it is perhaps a reasonable expectation that the results reported herein would be applicable to the situations where the temperature difference between the fluid and the cylinder is not too large, and one can justifiably use the physical properties at the mean fluid temperature. Also, the thermal dependence of the thermo-physical properties of the fluids (or of Prandtl number) varies from one substance to another, the present work elucidates the role of Prandtl number over a wide range of conditions rather than focusing on any specific fluids. This assumption allows the flow equations to be solved independently of the thermal energy equation. Under these conditions, the dimensionless governing equations in the Cartesian coordinates are given as:

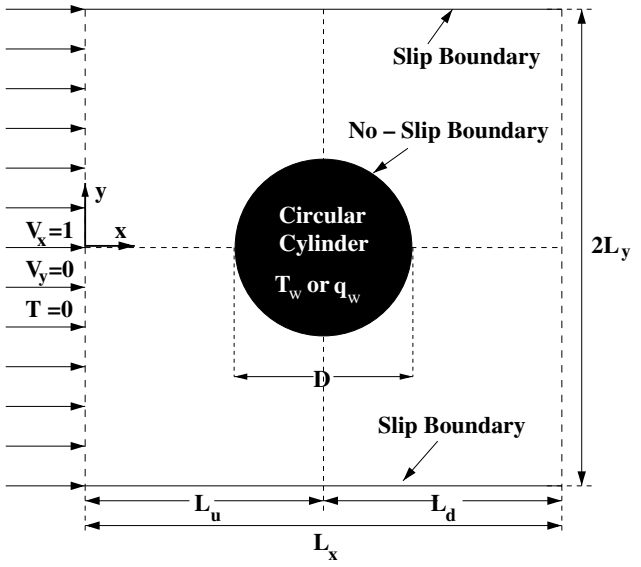

Fig. 1. Schematics of the unconfined flow around a circular cylinder.

Continuity equation

$$\frac{\partial V_x}{\partial x}+\frac{\partial V_y}{\partial y}=0 \tag{1}$$

x-component of the momentum equation

$$\frac{\mathrm{D}V_x}{\mathrm{D}t}=-\frac{\partial p}{\partial x}+\frac{1}{Re}\left(\frac{\partial \tau_{xx}}{\partial x}+\frac{\partial \tau_{yx}}{\partial y}\right) \tag{2a}$$

y-component of the momentum equation

$$\frac{\mathrm{D}V_y}{\mathrm{D}t}=-\frac{\partial p}{\partial y}+\frac{1}{Re}\left(\frac{\partial \tau_{yx}}{\partial x}+\frac{\partial \tau_{yy}}{\partial y}\right) \tag{2b}$$

Thermal energy equation

$$\frac{\mathrm{D}T}{\mathrm{D}t}=\frac{1}{RePr}\left(\frac{\partial^2 T}{\partial x^2}+\frac{\partial^2 T}{\partial y^2}\right) \tag{3}$$

The rheological equation of state for power-law fluids is given by

$$\tau_{ij}=2\eta\epsilon_{ij} \tag{4}$$

where $i,j=x,y$, and ϵ_{ij} are the components of the rate of strain tensor, related to the velocity field in the Cartesian coordinate, as follows:

$$\epsilon_{ij}=\frac{1}{2}\left(\frac{\partial V_i}{\partial j}+\frac{\partial V_j}{\partial i}\right) \tag{5}$$

The viscosity, η, is given by

$$\eta=(I_2/2)^{(n-1)/2} \tag{6}$$

where n is the power-law index (<1: shear-thinning; 1: Newtonian; and >1: shear-thickening fluids) and I_2 is the second invariant of the rate of strain tensor whose components are available in the standard texts, e.g. see Bird et al. [48].

Eqs. (1)–(6) have been rendered dimensionless using the following scaling variables: D for length variables, U_∞ for velocities, D/U_∞ for time, ρU_∞^2 for pressure, $m(U_\infty/D)^n$ for stress components, and $m(U_\infty/D)^{n-1}$ for viscosity, respectively. The temperature is non-dimensionalized by (T_w-T_∞) and $q_w\mathrm{D}/k$ for the CWT and UHF conditions, respectively. The dimensionless groups, namely, Reynolds number (Re) and Prandtl number (Pr), appearing in Eqs. (2) and (3) are defined as

$$Re=\frac{\rho D^n U_\infty^{2-n}}{m} \quad \text{and} \quad Pr=\frac{c_p m}{k}\left(\frac{U_\infty}{D}\right)^{n-1} \tag{7}$$

However, sometime it is customary to introduce the Peclet number ($Pe=Re\times Pr=\rho c_p U_\infty D/k$) which is independent of the power-law constants and thus offers the possibility of reconciling the results for Newtonian and power-law fluids.

After substituting Eq. (4) into Eq. (2), the conservative form of the non-dimensional governing equations (Eq. 2) can be written as

x-component

$$\frac{\mathrm{D}V_x}{\mathrm{D}t}=-\frac{\partial p}{\partial x}+\frac{\eta}{Re}\left(\frac{\partial^2 V_x}{\partial x^2}+\frac{\partial^2 V_x}{\partial y^2}\right)+\frac{2}{Re}\left(\epsilon_{xx}\frac{\partial \eta}{\partial x}+\epsilon_{yx}\frac{\partial \eta}{\partial y}\right) \tag{8a}$$

y-component

$$\frac{\mathrm{D}V_y}{\mathrm{D}t}=-\frac{\partial p}{\partial y}+\frac{\eta}{Re}\left(\frac{\partial^2 V_y}{\partial x^2}+\frac{\partial^2 V_y}{\partial y^2}\right)+\frac{2}{Re}\left(\epsilon_{xy}\frac{\partial \eta}{\partial x}+\epsilon_{yy}\frac{\partial \eta}{\partial y}\right) \tag{8b}$$

Thermal energy equation

$$\frac{\mathrm{D}T}{\mathrm{D}t}=\frac{1}{Pe}\left(\frac{\partial^2 T}{\partial x^2}+\frac{\partial^2 T}{\partial y^2}\right) \tag{9}$$

It is important to add here that the main thrust of the study is on steady solution, but the time-dependent terms are retained in Eqs. (8) and (9) because the false transient method has been used here to obtain the steady-state solution.

The physically realistic boundary conditions in dimensionless form for this flow may be written as follows.

- At the inlet boundary: Uniform flow

$$V_x=1, \quad V_y=0, \quad T=0 \quad \text{and} \quad \frac{\partial p}{\partial x}=0 \tag{10a}$$

- At the upper boundary: Slip flow

$$\frac{\partial V_x}{\partial y}=0, \quad V_y=0, \quad \frac{\partial T}{\partial y}=0 \quad \text{and} \quad \frac{\partial p}{\partial y}=0 \tag{10b}$$

- On the circular cylinder: No-slip flow

$$V_x = 0, \quad V_y = 0, \quad \frac{\partial p}{\partial n_s} = 0$$

and

$$\begin{cases} T = 1 & \text{(for CWT)} \\ \partial T/\partial n_s = -1 & \text{(for UHF)} \end{cases} \tag{10c}$$

where n_s represents the unit normal vector on the surface of the cylinder.

- At the exit boundary: The homogeneous Neumann boundary condition has been used:

$$\frac{\partial \phi}{\partial x} = 0 \quad \text{and} \quad p = p_\infty = 0 \tag{10d}$$

where, ϕ is a scalar (i.e., V_x, V_y and T).

- At the plane of symmetry, i.e., center line: Symmetric flow

$$\frac{\partial V_x}{\partial y} = 0, \quad V_y = 0, \quad \frac{\partial T}{\partial y} = 0 \quad \text{and} \quad \frac{\partial p}{\partial y} = 0 \tag{10e}$$

Owing to the symmetry, the solution is obtained only in the upper half of the domain in Fig. 1. The numerical solution of Eqs. (1), (8) and (9) along with the above-noted boundary conditions yield the velocity, pressure and temperature fields and these, in turn, are used further to obtain global characteristics like drag coefficients and Nusselt number, as described elsewhere [23,49]. The local Nusselt number on the surface of the circular cylinder is evaluated by the following expression:

$$Nu(\theta) = \frac{hD}{k} = \begin{cases} -(\partial T/\partial n_s) & \text{for CWT condition} \\ 1/T & \text{for UHF condition} \end{cases} \tag{11}$$

Such local values have been further averaged over the surface of a cylinder to obtain the surface averaged (or overall mean) Nusselt number as follows:

$$Nu = \frac{1}{2\pi} \int_0^\pi Nu(\theta)\, \mathrm{d}\theta \tag{12}$$

The average Nusselt number can be used in process engineering design calculations to estimate the rate of heat transfer from a cylinder in the CWT case, or to estimate the average surface temperature of the cylinder for the UHF condition. Dimensional analysis suggests the average Nusselt number to be a function of the Reynolds number, Prandtl or Peclet number, power-law index and the type of thermal boundary condition for the problem studied herein. This relationship is explored in this study.

4. Numerical solution methodology

Since a detailed description of the solution procedure and of the choice of numerical parameters is available elsewhere [23], only the salient features are recapitulated here. The governing equations have been discretized using the semi-implicit finite volume method [50] on a non-staggered and non-uniform grid, using the QUICK scheme [51–53] for convective terms and central difference scheme for other terms. The final equations were solved using a Gauss-Seidel iterative algorithm. The steady-state solution has been obtained using the false transient method. A zero-volume cell at each boundary condition has been used to implement the boundary conditions exactly at the surface of the cylinder. The fully converged velocity field [23] was used as the input to the thermal energy equation. The resulting temperature field is used to deduce the values of the local and average Nusselt number on the surface of the cylinder. The results presented in this work are based on a domain size $L_u = L_d = L_y = 30.5D$ for all values of Re and n, and grid size, $M \times N$:

$$101 \times 283 \quad \text{for} \quad \begin{cases} n \geqslant 0.8; & 5 \leqslant Re \leqslant 10 \\ n \geqslant 0.65; & 15 \leqslant Re \leqslant 40 \end{cases}$$

$$61 \times 176 \quad \text{for} \quad \begin{cases} n < 0.8; & 5 \leqslant Re \leqslant 10 \\ n < 0.65; & 15 \leqslant Re \leqslant 40 \end{cases}$$

where M and N are the number of grid points on the half surface of the cylinder and on the symmetry line in the upstream/downstream sections, respectively. A thorough justification for these choices of the numerical parameters has been provided in our previous studies [23,49].

5. Results and discussion

Extensive numerical results have been obtained by systematically varying the value of the Reynolds number in the range as $5 \leqslant Re \leqslant 40$, in the steps of 5, and the power-law index in the range $0.6 \leqslant n \leqslant 2.0$, in the steps of 0.1 for $n < 1$ and in the steps of 0.2 for $n > 1$, and the Prandtl number, $Pr = 1$, 5, 10, 20, 50, 100, 200, 500 and 1000 for the two thermal boundary conditions on the surface of the cylinder. The maximum value of the Peclet number was, however, limited to 5000, i.e., $Pe \leqslant 5000$ therefore the range of Prandtl number is linked to the value of the Reynolds number.

5.1. Validation of results

The numerical methodology used in this work has been validated extensively for the flow characteristics of power-law fluids [23] and for heat transfer characteristics of Newtonian fluid [49], all of which show excellent correspondence with the literature values. While the present heat transfer results for Newtonian fluids are within 2–3% of the previous numerical results and within 10% of the experimental values, as detailed in Bharti et al. [49], the present results for power-law fluids are compared with the only study available in the literature [22] in Table 1. An examination of Table 1 reveals that the present results are generally within ±5% of the literature values, the agreement is

Table 1
Comparison of the average Nusselt number ($Pr = 1$) with the literature values for power-law fluids

Re	Source	CWT Condition				UHF Condition			
		$n = 0.8$	1	1.2	1.4	0.8	1	1.2	1.4
5	Present	1.684	1.586	1.532	1.501	1.829	1.700	1.631	1.591
	Soares et al. [22]	1.621	1.590	1.566	1.548	1.735	1.693	1.661	1.637
10	Present	2.227	2.087	2.002	1.948	2.494	2.309	2.197	2.125
	Soares et al. [22]	2.116	2.058	2.011	1.973	2.340	2.259	2.197	2.146
20	Present	2.974	2.771	2.639	2.546	3.409	3.147	2.973	2.854
	Soares et al. [22]	2.799	2.696	2.613	2.545	3.182	3.048	2.931	2.840
30	Present	3.529	3.279	3.110	2.988	4.082	3.763	2.546	3.389
	Soares et al. [22]	3.309	3.171	3.060	2.969	3.807	3.622	3.474	3.354
40	Present	3.992	3.703	3.502	3.352	4.635	4.274	4.019	3.827
	Soares et al. [22]	3.736	3.570	3.435	3.325	4.325	4.104	3.926	3.781

somewhat better for $n > 1$ than that for $n < 1$. Deviations of this order are not at all uncommon in numerical studies and arise due to the differences in the flow schematics, problem formulations, grid and/or domain sizes, discretization schemes, numerical methods, etc. For instance, some of the discrepancies seen in Table 1 can be ascribed to the cylinder-in-cylinder domain and to the slightly different discretization used by Soares et al. [22]. In comparing the results shown in Table 1, it should be borne in mind that owing to the non-linear viscous terms, the numerical values for power-law fluids are known to be less accurate than the corresponding values for Newtonian fluids. Thus, owing to such variations inherent in numerical solutions, it is virtually impossible to estimate the accuracy of the results. But based on our past extensive experience and on the validation shown elsewhere [23,49] and in Table 1 here, the present results are believed to be reliable to within $\pm 2 - 3\%$ of the mean of the two values reported in Table 1.

5.2. Heat transfer results

The dependence of the local Nusselt number on the surface of the cylinder, of the Nusselt number at the stagnation points and of the average Nusselt number on *Re*, *Pr* and *n* for the two thermal boundary conditions is presented and discussed in the ensuing sections. The average Nusselt number values have also been interpreted in terms of Colburn heat transfer factor, *j*.

5.2.1. Variation of local Nusselt number on the surface of the cylinder

Figs. 2 and 3 show the representative variation of the local Nusselt number, $Nu(\theta)$ on the surface of the cylinder with Reynolds and Prandtl numbers and power-law index at Reynolds number of 5 ($1 \leqslant Pr \leqslant 1000$) and 40 ($1 \leqslant Pr \leqslant 100$), power-law index of 0.6, 1 and 2 and for both CWT (solid lines) and UHF (broken lines) thermal boundary conditions, respectively. While these figures show qualitatively similar behaviour of the Nusselt number over the surface of the cylinder, but a complex interplay between the flow behaviour index (n) and kinematic parameters (Re, Pr) is observed in quantitative terms. At low Reynolds and/or Prandtl number, the local values of the Nusselt number show little variation over the surface from $\theta = 0$ to $\theta = \pi$. This is due to the fact that at such low Reynolds numbers, the heat transfer occurs primarily by conduction, with a little convection, irrespective of the type of the thermal boundary condition on the surface of the cylinder and power-law index. This finding is also consistent with heat/mass transfer in power-law fluids from beds of spherical particles [43,54–56] and from tube banks [19,47]. As the Prandtl number and/or Reynolds number is gradually increased, the contribution of convection increases and the Nusselt number is seen to vary over the surface of the cylinder.

The value of the local Nusselt number in the front of the cylinder increases with an increase in the shear-thinning behaviour (i.e., decrease in the value of n below unity), while it decreases with an increase in the shear-thickening behaviour for both thermal boundary conditions. The value of θ at which the maximum in Nusselt number occurs can be seen to decrease with an increase in Reynolds number for $n < 1$. On the other hand, in the rear of the cylinder, the Nusselt number decreases all the way up to $\theta = \pi$ when there is no flow separation, e.g. see Fig. 2(a)–(b), and up to $\theta = \theta_s$ (the separation angle) in a separated flow, e.g. see Figs. 2(c) and 3(a)–(c). The Nusselt number also increases in the recirculating region in both shear-thinning and shear-thickening fluids. The isoflux boundary condition results in a somewhat greater value of the Nusselt number than that for the isothermal condition in shear-thickening/Newtonian fluid behaviours in the front of the cylinder; however, the opposite behaviour is seen in shear-thinning fluids. The Nusselt number was always seen to be higher for the isoflux condition than that for isothermal condition in the rear of the cylinder at low Reynolds numbers; this trend is however reversed at high Reynolds numbers. Also, the Nusselt number is seen to be larger in shear-thinning fluids than that in Newtonian and in shear-thickening fluids. Thus, shear-thinning promotes heat transfer whereas shear-thickening seem to impede it.

5.2.2. Nusselt number at the stagnation points

Qualitatively similar dependence of the Nusselt number at the front stagnation ($\theta = 0$) point, $Nu(0)$ (Fig. 4(a)) and at the rear stagnation ($\theta = \pi$) point, $Nu(\pi)$ (Fig. 4(b)) can

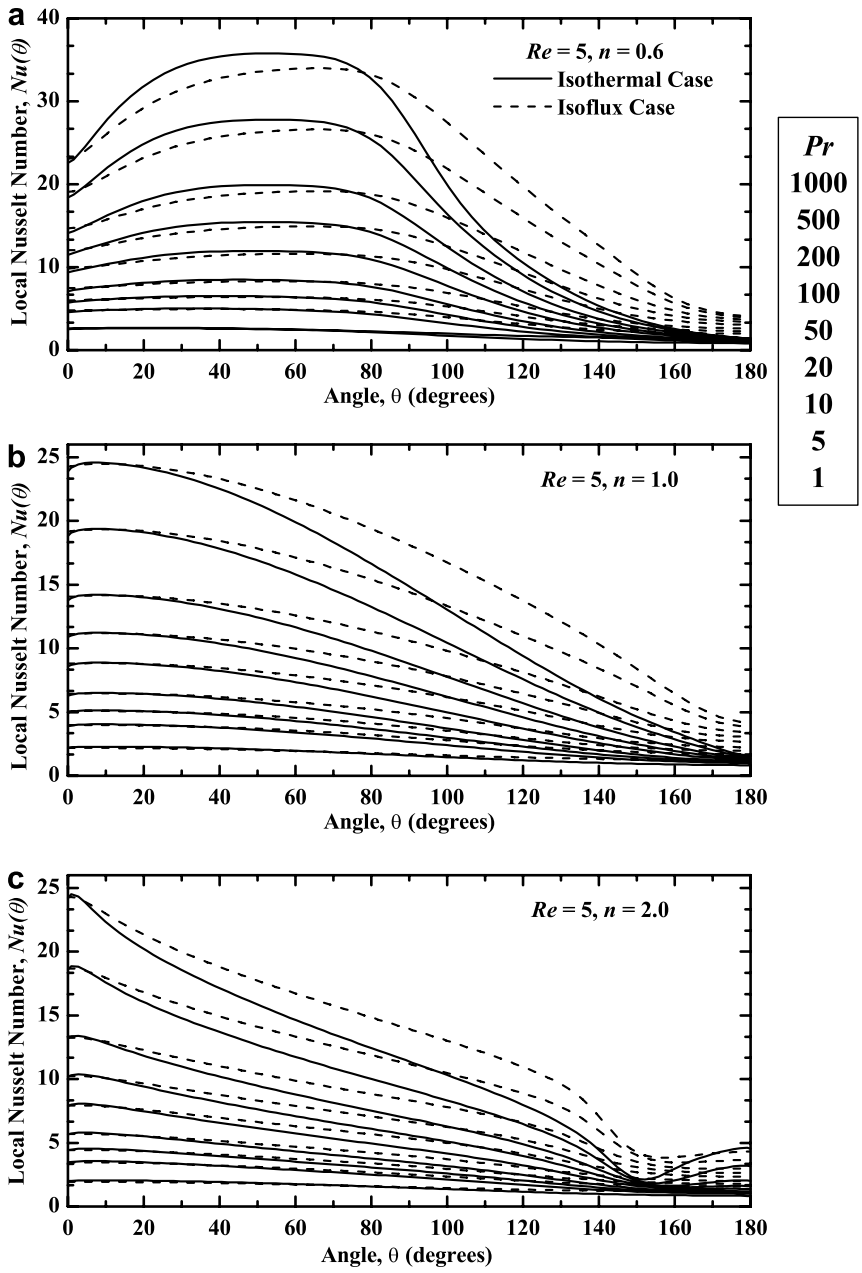

Fig. 2. Dependence of distribution of the local Nusselt number, $Nu(\theta)$ over the surface of the cylinder on Pr and n for $Re = 5$ under CWT (–) and UHF (– –) condition.

be seen on the Reynolds number, Prandtl number and power-law index for both thermal boundary conditions. At low Reynolds and/or Prandtl numbers, the front stagnation Nusselt number shows little or no variation with the power-law index. The variation, however, increases with an increase in the value of the Reynolds and/or Prandtl numbers. As the level of shear-thinning ($n < 1$) increases, the value of $Nu(0)$ increases, the opposite dependence of flow behaviour index can be seen in the shear-thickening ($n > 1$) fluids. The dependence of the Nusselt number at the front stagnation point on the Re, Pr and n can be represented by the following correlation:

$$Nu(0) = F(n)Re^{c}Pr^{d} \quad \text{where} \quad F(n) = a^{n}\Delta^{b} \quad \text{and} \quad \Delta = \left(\frac{3n+1}{4n}\right) \tag{13}$$

The values of a, b, c, d and the resulting average and maximum deviations of the numerical data from Eq. (13) are shown in Table 2. Admittedly, the maximum deviation of ~15% may appear large, but considering the wide ranges of the Reynolds and Prandtl numbers and of the power-law index, it is regarded to be acceptable.

The value of the Nusselt number at the rear stagnation point, $Nu(\pi)$ shows a complex dependence on the Reynolds and Prandtl numbers and power-law index (Fig. 4(b)). This

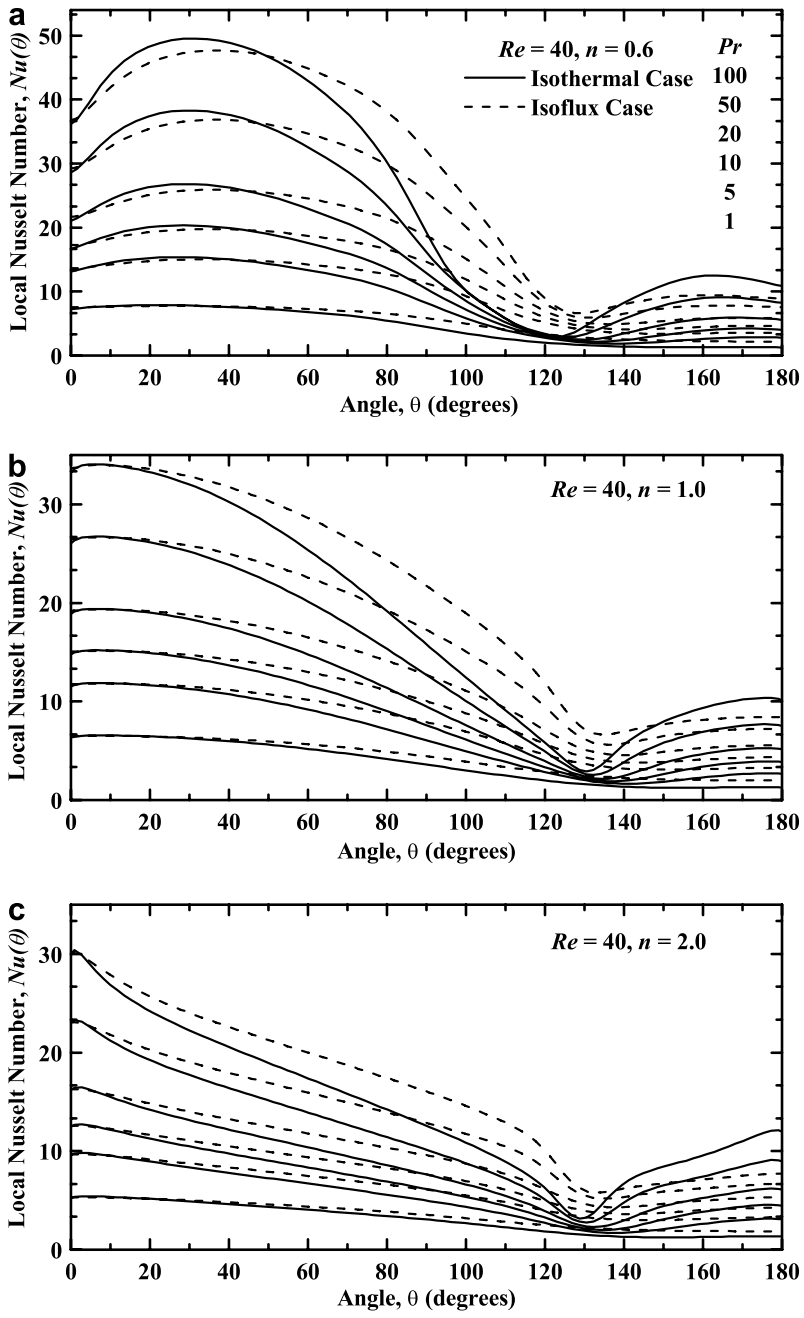

Fig. 3. Dependence of distribution of the local Nusselt number, $Nu(\theta)$ over the surface of the cylinder on Pr and n for $Re = 40$ under CWT (–) and UHF (– –) condition.

dependence is clearly influenced by the varying levels of recirculation behind the cylinder. Flow separation does not occur in shear-thinning fluids at $Re = 5$ [23] whereas it can clearly be seen in shear-thickening fluids at this value of the Reynolds number. At low Reynolds and/or Prandtl numbers, the Nusselt number corresponding to the rear stagnation is seen to be independent of the power-law index. Furthermore, the value of $Nu(\pi)$ is seen to vary a little with the Prandtl number and/or the power-law index in the absence of separation (Fig. 4(b)) for the CWT condition, whereas significant dependence of $Nu(\pi)$ on the Prandtl number is seen for the UHF condition (Fig. 4(b)). The value of $Nu(\pi)$ in shear-thickening fluids is seen to increase with an increase in Reynolds and/or Prandtl number and/or power-law index for both thermal boundary conditions; however, the UHF boundary condition shows a lower value of $Nu(\pi)$ than that for the CWT condition.

5.2.3. Average Nusselt number, Nu

Owing to the underlying differences in the two thermal boundary conditions on the surface of the cylinder, the results (Fig. 5(a) and (b)) are discussed separately.

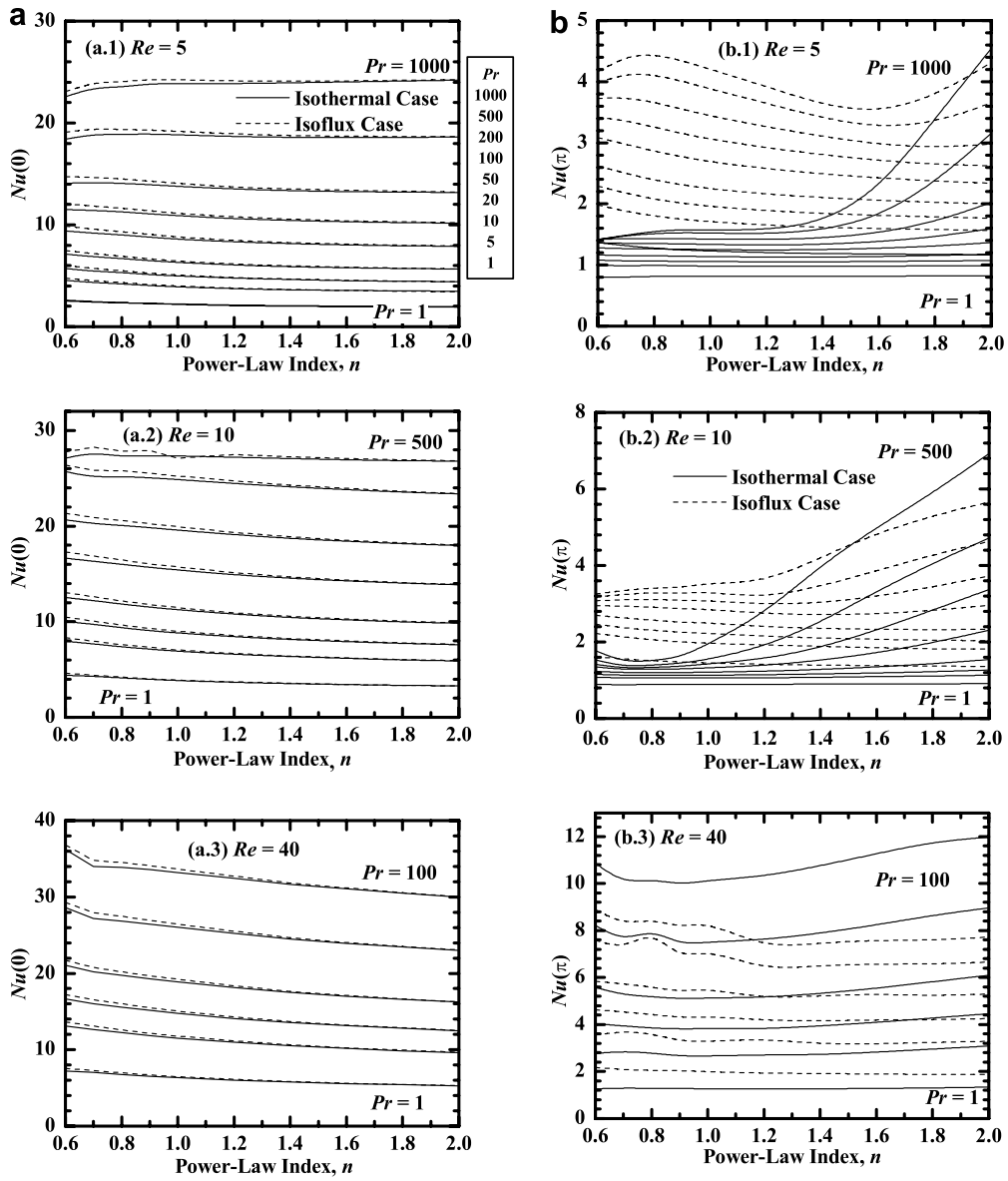

Fig. 4. Effect of *Re*, *Pr* and *n* on $Nu(\theta)$, the Nusselt number at the (a) front ($\theta = 0$) and (b) rear ($\theta = \pi$) stagnation points of the cylinder for CWT (–) and UHF (– –) boundary conditions.

(a) *CWT Condition*: The dependence of the average Nusselt number on the Reynolds and Prandtl numbers and power-law index for the CWT condition is shown in Fig. 5(a). For a fixed value of the Reynolds number, the average Nusselt number increases with a gradual increase in Prandtl number, irrespective of the value of the fluid behaviour index, n. The shear-thinning fluids ($n < 1$) show a higher rate of enhancement in heat transfer with an increase in the Prandtl number, which decreases as the fluid behaviour changes to Newtonian ($n = 1$) and finally, to shear-thickening ($n > 1$). For a fixed value of the power-law index, the value of average Nusselt number increases with a gradual increase in Prandtl number and/or Reynolds number and/or both. For instance, at $Pr = 1$ the value of the Nusselt number increases from 1.863 to 4.478 at $n = 0.6$ and from 1.458 to 3.089 at $n = 2$ as *Re* is increased from 5 to 40, whereas at $Pr = 100$, it increases from 9.615 to 25.505 and from 5.534 to 14.388 at $n = 0.6$ and 2, respectively.

(b) *UHF Condition*: The effects of the Reynolds number, Prandtl number and power-law index on the average Nusselt number for the uniform heat flux (UHF) condition are seen (Fig. 5(b)) to be qualitatively similar as above, though the actual difference between the two values is somewhat dependent on the values of the Reynolds and Prandtl numbers and of the power-law index. The value of the average Nusselt number is always higher under the UHF condition than that for CWT condition. For instance, the two values of the Nusselt number differ by a maximum of ~18% for $n = 1.4$, $Re = 5$ and $Pr = 500$.

Table 2
Functional parameters for the dependence of the Nusselt number and *j*-factor on the Reynolds number (*Re*), Prandtl number (*Pr*), power-law index (*n*) and on the thermal boundary conditions

	$Nu(0)$ (CWT)	$Nu(0)$ (UHF)	Nu (CWT)	Nu (UHF)	j (CWT)	j (UHF)
a	0.932	0.947	0.052	0.146	0.761	0.861
b	0.229	0.400	0.091	0.104	0.413	0.413
c	0.532	0.533	0.246	0.226	0.561	0.556
d	0.348	0.347	2.552	2.161	–	–
e	–	–	0.495	0.483	–	–
f	–	–	0.032	0.049	–	–
g	–	–	0.721	0.704	–	–
ℓ	–	–	0.119	0.102	–	–
δ_{avg} (%)	2.92	3.13	2.32	1.22	3.80	2.82
δ_{max} (%)	14.71	15.68	17.00	9.69	20.46	13.80

δ: relative r.m.s. deviation from the numerical data (Total # of data points = 560).

The functional dependence of the average Nusselt number on the Reynolds and Prandtl numbers and the power-law index for both conditions can be best represented by the following correlation:

$$Nu = F(n)Re^{e/(fn+1)}Pr^{g/(\ell n+2)}$$

$$\text{where} \quad F(n) = a^{(-bn+c)}\Delta^{d} \tag{14}$$

The values of the constants a, b, c, d, e, f, g and ℓ appearing in Eq. (14), together with the maximum and average deviations are summarized in Table 2 for both thermal boundary conditions. An excellent agreement can be seen (Fig. 6(a)) between the present numerical data and the predictions of Eq. (14) for both isothermal and isoflux boundary conditions.

5.2.4. Colburn *j*-factor

Some further attempts have been made to establish the functional relationship between the Reynolds, Prandtl and average Nusselt numbers by introducing the Colburn heat transfer factor, j defined as

$$j = \frac{Nu}{RePr^{1/3}} \tag{15}$$

The main virtue of this parameter lies in the fact that it affords the possibility of reconciling the results for a range of Reynolds and Prandtl numbers into a single curve. The present numerical data for the *j*-factor can be best represented by the following correlation

$$j = \frac{a}{n^{b}Re^{c}} \tag{16}$$

The best values of the fitted constants in Eq. (16) together with the average and maximum deviations from the numerical data are shown in Table 2. Fig. 6(b) shows a comparison between the numerical values of j and the predictions of proposed Eq. (16).

5.3. Comparison with experimental results

Limited experimental results are available for heat/mass transfer from cylinders in power-law fluids, but most of these either relate to viscoelastic liquids [41,57] or to the values of the Reynolds number and/or Prandtl number which are beyond the range of conditions covered in this study, thereby eliminating the possibility of direct comparisons, except for the limited results reported in Ghosh et al. [36]. Based on the limited mass transfer data from cylinders in power-law fluids ($0.0018 \leqslant Re \leqslant 513$; $0.72 \leqslant n \leqslant 1.0$) from a cylinder, Ghosh et al. [35,36] presented the following correlation

$$Nu = \alpha Re^{\left(\beta+\frac{(n-1)}{3(n+1)}\right)}Pr^{1/3} \tag{17}$$

$$\alpha = \begin{cases} 2.260\,(\beta = 1/3) & \text{for } Re \leqslant 10 \\ 0.785\,(\beta = 1/2) & \text{for } Re \geqslant 10 \end{cases}$$

and reported the average deviation of ±7.5%, though the maximum errors of 35–40% are evident in their paper.

A comparison between the present numerical results and the predictions of Eq. (17) is shown in Fig. 7. In assessing this comparison, it must be borne in mind that the present results are based on the assumptions of infinitely long circular cylinder and constant fluid properties whereas the L/D ratio for the cylinders used in experimental studies is of the order of 2. Furthermore, there will always be, however small, wall effects present in experimental results which are neglected in numerical simulations. The wall effects also tend to yield somewhat higher values of the Nusselt number than that under unconfined condition and the trends seen in Fig. 7 corroborate this assertion. Furthermore, the mass transfer results are obtained by the weight loss method and therefore the size (and possibly shape) of the test specimen is continuously changing. These factors coupled with the fact that there is virtually no overlap in terms of the values of the Schmidt number associated with Eq. (17) and that of Prandtl number in the present numerical work, are probably responsible for the discrepancies seen in Fig. 7, albeit these are of the same order as the uncertainty of the experiments. But nonetheless Eq. (17) does capture qualitatively the dependence of the Nusselt number on the Reynolds and Prandtl numbers, and therefore the comparison shown in Fig. 7 should be interpreted qualitatively rather than quantitatively.

From an engineering point of view, it is also appropriate to make some general remarks about the utility of the results reported herein. Admittedly, the thermo-physical properties, notably, power-law consistency index of the fluids does vary with the temperature, hence, it is worthwhile to assess the impact of this assumption. Eq. (14) can be rearranged to show that

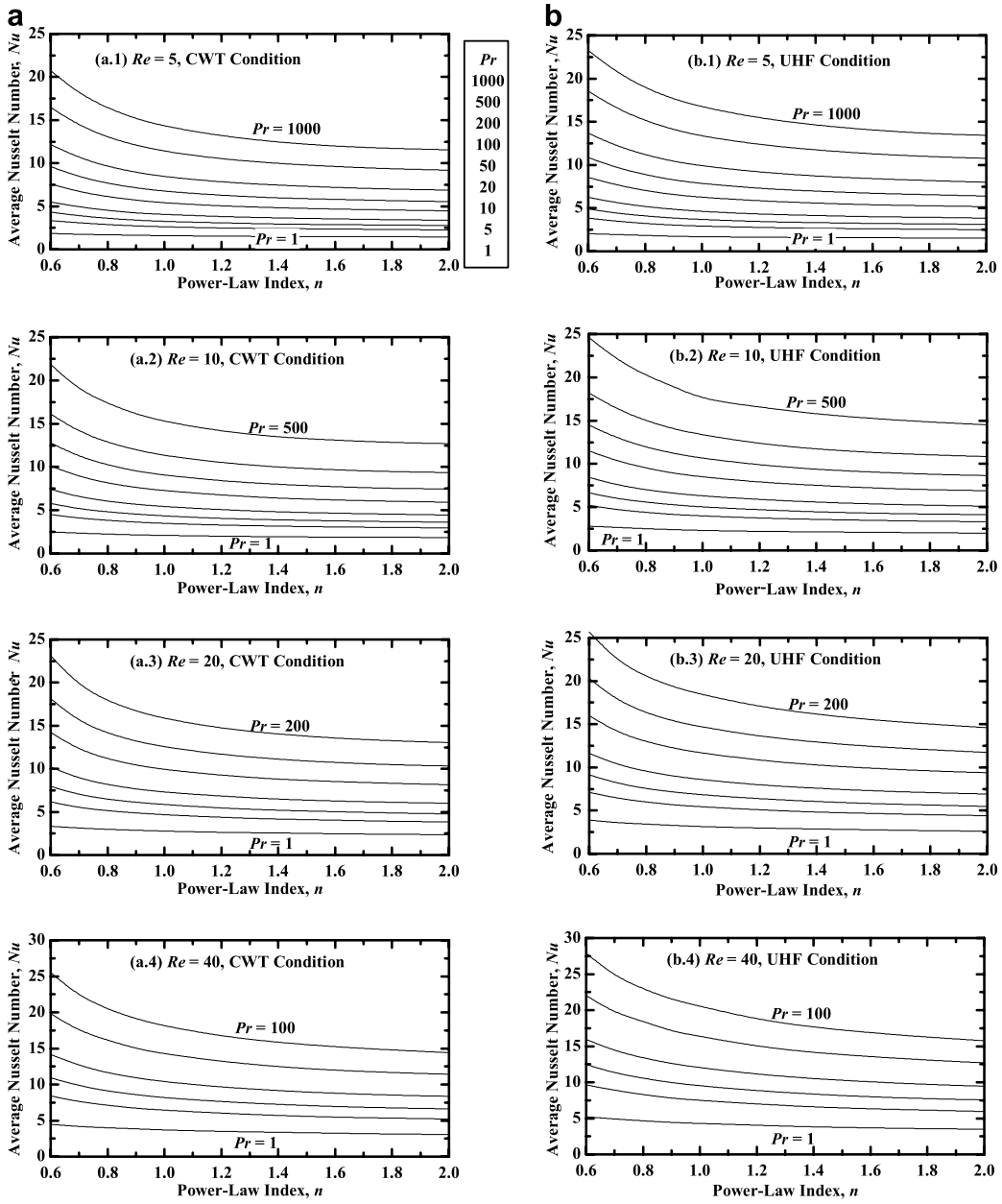

Fig. 5. Dependence of the average Nusselt number (Nu) on Re, Pr and n for (a) CWT and (b) UHF conditions.

$$Nu \propto \eta_{\text{eff}}^{\lambda} \quad \text{where} \quad \lambda = \left[\frac{g}{(\ell n+2)} - \frac{e}{(fn+1)}\right]$$

Using the value of e, f, g, ℓ, etc. presented in Table 2, it can readily be shown that the value of $\lambda \approx 0.14$ in the range $0.6 \leqslant n \leqslant 2$. Thus, even a 100% change in the value of the effective viscosity (η_{eff}) due to temperature variation will alter the value of Nusselt number by 10%. Therefore, it appears that the assumption of the temperature independent thermo-physical properties of fluids used in this work is not as bad as it seems. The results presented herein can thus be used when a moderate variation in thermo-physical properties is encountered by using the physical properties evaluated at the mean temperature. In case of appreciable variation in the values of the effective viscosity due to temperature-dependent properties, one can perhaps use the same correction as that used for Newtonian fluids, i.e., $(\eta_s/\eta_w)^{0.14}$, atleast as a first order approximation. In case of large variations, however, one must solve the coupled non-linear differential equations which further adds to the computational difficulties even in Newtonian fluids, as is reflected by the lack of such results in the literature even for air and water. Also, it is important to mention here that many materials of industrial significance exhibit the value of power-law index as low as 0.3–0.4. Owing to the increasing degree of non-linearity of the viscous term, such small values of n pose enormous convergence problems, as also reported by others [20,58].

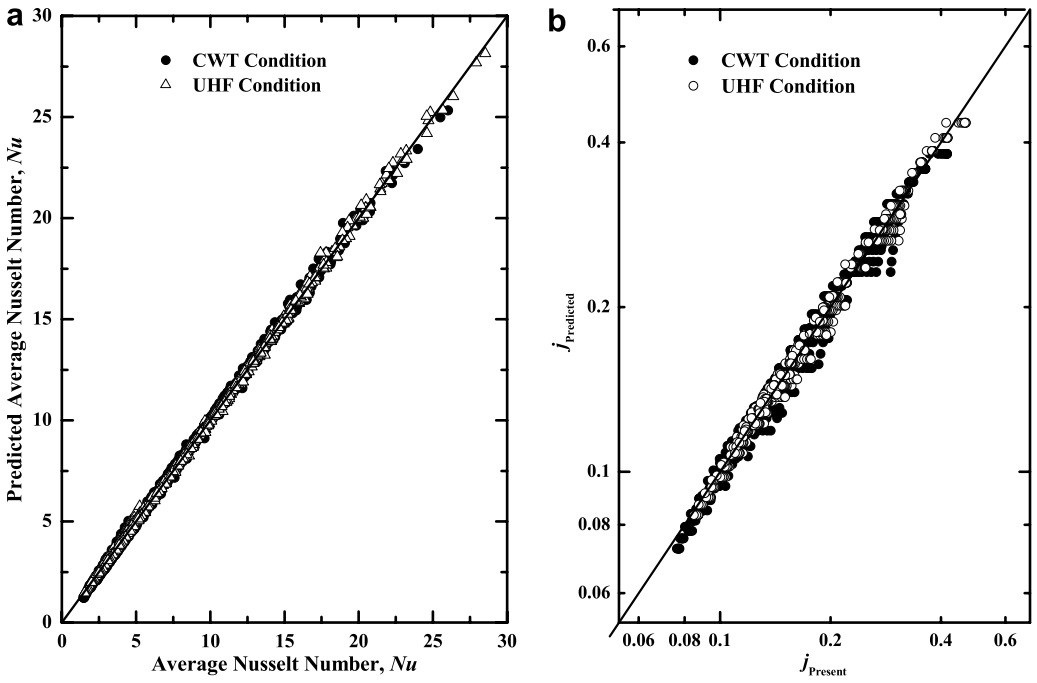

Fig. 6. Comparison (a) average Nusselt number: present vs. predictions of Eq. (14) and (b) *j*-factor: present (Eq. (15)) vs. predictions of Eq. (16).

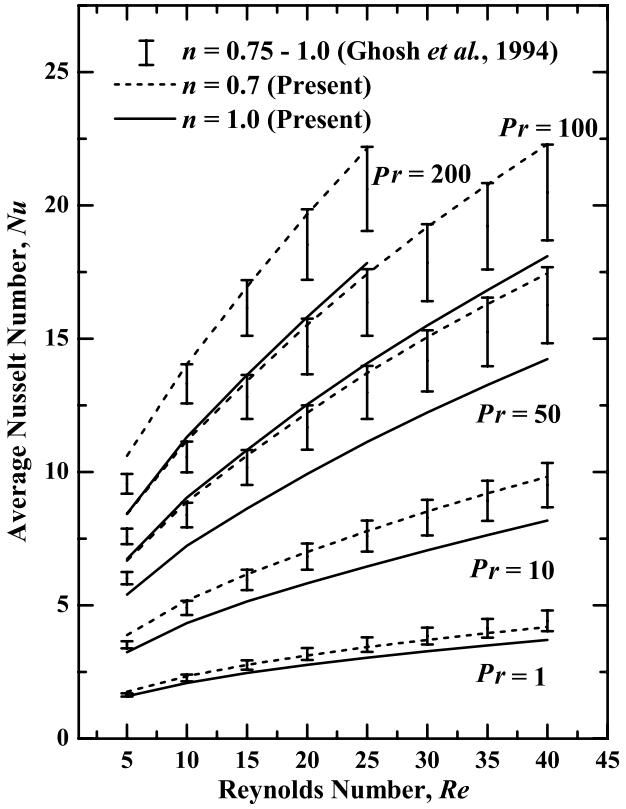

Fig. 7. Comparison between present numerical results and experimental results.

Therefore, it is worthwhile to explore the possibility of other methods for such small values of power-law index.

6. Conclusions

The forced convection heat transfer in cross-flow of power-law fluids from an unconfined circular cylinder has been numerically investigated using FVM and the QUICK scheme in conjunction with a non-uniform grid for the range of Reynolds number ($5 \leqslant Re \leqslant 40$), power-law index ($0.6 \leqslant n \leqslant 2.0$) and Prandtl number ($1 \leqslant Pr \leqslant 1000$) in the steady flow regime. The local Nusselt number in the front side of the cylinder decreases as the fluid behaviour changes from shear-thinning to shear-thickening fluids and/or as the Prandtl number is decreased, irrespective of the value of the Reynolds number and the type of the thermal boundary condition. The minimum local value was seen to occur near the point of separation, which again increases in the recirculating region. The Nusselt number values at the front stagnation point show very weak dependence on the power-law index and thermal boundary conditions, as opposed to that at the rear stagnation point. The shear-thinning fluids ($n < 1$) show higher heat transfer than that for Newtonian ($n = 1$) and shear-thickening fluids ($n > 1$). Also, the average Nusselt number increases with an increase in the Reynolds number and/or Prandtl number and/or both, irrespective of the type of fluid behaviour. The functional dependence of the present numerical results on the kinematic parameters (Re, Pr) and on the power-law index have also been presented.

References

[1] R.A. Ahmad, Steady-state numerical solution of the Navier–Stokes and energy equations around a horizontal cylinder at moderate

Reynolds numbers from 100 to 500, Heat Transfer Eng. 17 (1996) 31–81.
[2] R.P. Chhabra, Bubbles, Drops and Particles in Non-Newtonian Fluids, second ed., CRC Press, Boca Raton, FL, 2006.
[3] R.P. Chhabra, Hydrodynamics of non-spherical particles in non-newtonian fluids, in: N.P. Cheremisinoff, P.N. Cheremisinoff (Eds.), Handbook of Applied Polymer Processing Technology, Marcel Dekker, New York, 1996, Chapter 1.
[4] R.P. Chhabra, Heat and mass transfer in rheologically complex systems, in: D. Singer, D. De Kee, R.P. Chhabra (Eds.), Advances in the Rheology and Flow of Non-Newtonian Fluids, Elsevier, Amsterdam, 1999, Chapter 39.
[5] R. Clift, J. Grace, M.E. Weber, Bubbles, Drops and Particles, Academic Press, New York, USA, 1978.
[6] C.F. Lange, F. Durst, M. Breuer, Momentum and heat transfer from cylinders in laminar crossflow at $10^{-4} \leqslant Re \leqslant 200$, Int. J. Heat Mass Transfer 41 (1998) 3409–3430.
[7] V.T. Morgan, The overall convective heat transfer from smooth circular cylinders, Adv. Heat Transfer 11 (1975) 199–264.
[8] C.H.K. Williamson, Vortex dynamics in the cylinder wake, Ann. Rev. Fluid Mech. 28 (1996) 477–539.
[9] M.M. Zdravkovich, Flow Around Circular Cylinder vol. 1, Fundamentals, Oxford University Press, New York, USA, 1997.
[10] M.M. Zdravkovich, Flow Around Circular Cylinder vol. 2, Applications, Oxford University Press, New York, USA, 2003.
[11] A. Zukauskas, Convective heat transfer in cross flow, in: A. Zukauskas, S. Kakac, R.K. Shah, W. Aung (Eds.), Handbook of Single-Phase Convective Heat Transfer, Wiley, New York, USA, 1987, pp. 6.1–6.45.
[12] P.J. Carreau, D. De Kee, R.P. Chhabra, Rheology of Polymeric Systems, Hanser-Gardner: Munich, Germany, 1997.
[13] R.P. Chhabra, J.F. Richardson, Non-Newtonian Flow in the Process Industries: Fundamentals and Engineering Applications, Butterworth-Heinemann, Oxford, 1999.
[14] K.K. Talwar, B. Khomani, Flow of viscoelastic fluids past periodic square arrays of cylinders: inertial and shear-thinning viscosity and elasticity effects, J. Non-Newtonian Fluid Mech. 57 (1995) 177–202.
[15] A.W. Liu, D.E. Bornside, R.C. Armstrong, R.A. Brown, Viscoelastic flow of polymer solutions around a periodic, linear array of cylinders: comparisons of predictions for microstructure and flow field, J. Non-Newtonian Fluid Mech. 77 (1998) 153–190.
[16] R.I. Tanner, Stokes paradox for power-law flow around a cylinder, J. Non-Newtonian Fluid Mech. 50 (1993) 217–224.
[17] E. Marusic-Paloka, On the Stokes paradox for power-law fluids, Z. Angew. Math. Mech. 81 (2001) 31–36.
[18] M.J. Whitney, G.J. Rodin, Force-velocity relationships for rigid bodies translating through unbounded shear-thinning power-law fluids, Int. J. Non-Linear Mech. 36 (2001) 947–953.
[19] J.M. Ferreira, R.P. Chhabra, Analytical study of drag and mass transfer in creeping power-law flow across tube banks, Ind. Eng. Chem. Res. 43 (2004) 3439–3450.
[20] S.J.D. D'Alessio, J.P. Pascal, Steady flow of a power-law fluid past a cylinder, Acta Mech. 117 (1996) 87–100.
[21] R.P. Chhabra, A.A. Soares, J.M. Ferreira, Steady non-Newtonian flow past a circular cylinder: a numerical study, Acta Mech. 172 (2004) 1–16.
[22] A.A. Soares, J.M. Ferreira, R.P. Chhabra, Flow and forced convection heat transfer in cross flow of non-Newtonian fluids over a circular cylinder, Ind. Eng. Chem. Res. 44 (2005) 5815–5827.
[23] R.P. Bharti, R.P. Chhabra, V. Eswaran, Steady flow of power-law fluids across a circular cylinder, Can. J. Chem. Eng. 84 (2006) 406–421.
[24] S.J.D. D'Alessio, L.A. Finlay, Power-law flow past a cylinder at large distances, Ind. Eng. Chem. Res. 43 (2004) 8407–8410.
[25] P. Sivakumar, R.P. Bharti, R.P. Chhabra, Effect of power-law index on critical parameters for power-law flow across an unconfined circular cylinder, Chem. Eng. Sci. 61 (2006) 6035–6046.
[26] J.-P. Hsu, C.-F. Shie, S. Tseng, Sedimentation of a cylindrical particle in a Carreau fluid, J. Colloid Interface Sci. 286 (2005) 392–399.
[27] M.J. Shah, E.E. Peterson, A. Acrivos, Heat transfer from a cylinder to a power-law non-Newtonian fluid, AICHE J. 8 (1962) 542–549.
[28] R.W. Serth, K.M. Kiser, A solution of 2-dimensional boundary-layer equations for an Ostwald-de Waele fluid, Chem. Eng. Sci. 22 (1967) 945–956.
[29] T. Mizushina, H. Usui, Approximate solution of the boundary layer equations for the flow of a non-Newtonian fluid around a circular cylinder, Heat Transfer Jap. Res. 7 (1978) 83–92.
[30] T.-Y. Wang, C. Kleinstreuer, Local skin friction and heat transfer in combined free-forced convection from a cylinder or sphere to a power-law fluid, Int. J. Heat Fluid Flow 9 (1988) 182–187.
[31] W.A. Khan, J.R. Culham, M.M. Yovanovich, Fluid flow and heat transfer in power-law fluids across circular cylinders—analytical study, J. Heat Transfer 128 (2006) 870–878.
[32] K. Takahashi, M. Maeda, S. Ikai, Experimental study on heat transfer from a cylinder submerged in a non-Newtonian fluid, Die dem Nahenungsansatz von K. Pohlhausen genugen, Lilenthal Bericht, 510, 1977, pp. 335–339.
[33] T. Mizushina, H. Usui, K. Veno, T. Kato, Experiments of pseudoplastic fluid cross flow around a circular cylinder, Heat Transfer Jap. Res. 7 (1978) 92–101.
[34] S. Kumar, B.K. Mall, S.N. Upadhyay, On the mass transfer in non-Newtonian fluids: II Transfer from cylinders to power-law fluids, Lett. Heat Mass Transfer 7 (1980) 55–64.
[35] U.K. Ghosh, S.N. Gupta, S. Kumar, S.N. Upadhyay, Mass transfer in cross flow of non-Newtonian fluids around a circular cylinder, Int. J. Heat Mass Transfer 29 (1986) 955–960.
[36] U.K. Ghosh, S.N. Upadhyay, R.P. Chhabra, Heat and mass transfer from immersed bodies to non-Newtonian fluids, Adv. Heat Transfer 25 (1994) 251–319.
[37] B.K. Rao, Heat transfer to non-Newtonian flows over a cylinder in cross flow, Int. J. Heat Fluid Flow 21 (2000) 693–700.
[38] P.M. Coelho, F.T. Pinho, A.H. Rodrigues, Flow of shear-thinning fluids around a cylinder: vortex shedding and drag characteristics, 8th International Symposium on Applications of Laser Techniques to Fluid Mechanics, July 8–11, Lisbon, Portugal, vol. II, 1996, 35.5.1–35.5.8.
[39] P.M. Coelho, F.T. Pinho, Vortex shedding in cylinder flow of shear-thinning fluids. I. Identification and demarcation of flow regime, J. Non-Newtonian Fluid Mech. 110 (2003) 143–176;
Also see P.M. Coelho, F.T. Pinho, Vortex shedding in cylinder flow of shear-thinning fluids. II. Flow characteristics, J. Non-Newtonian Fluid Mech. 110 (2003) 177–193.
[40] P.M. Coelho, F.T. Pinho, Vortex shedding in cylinder flow of shear-thinning fluids. III. Pressure measurements, J. Non-Newtonian Fluid Mech. 121 (2004) 55–68.
[41] K. Ogawa, C. Kuroda, I. Inoue, Forced-convective mass transfer in viscoelastic fluid around a sphere and a cylinder, J. Chem. Eng. Jap. 17 (1984) 654–656.
[42] D. Rodrigue, R.P. Chhabra, D. De Kee, Drag on non-spherical particles in non-Newtonian fluids, Can. J. Chem. Eng. 72 (1994) 588–593.
[43] R.P. Chhabra, J. Comiti, I. Machac, Flow of non-Newtonian fluids in fixed and fluidized beds: a review, Chem. Eng. Sci. 56 (2001) 1–27.
[44] A.K. Gupta, A. Sharma, R.P. Chhabra, V. Eswaran, Two-dimensional steady flow of a power-law fluid past a square cylinder in a plane channel: momentum and heat transfer characteristics, Ind. Eng. Chem. Res. 42 (2003) 5674–5686.
[45] B. Paliwal, A. Sharma, R.P. Chhabra, V. Eswaran, Power-law fluid flow past a square cylinder: momentum and heat transfer characteristics, Chem. Eng. Sci. 58 (2003) 5315–5329.
[46] S.D. Dhole, R.P. Chhabra, V. Eswaran, Forced convection heat transfer from a sphere to non-Newtonian power law fluids, AICHE (2006) in press, doi:10.1002/aic.10983.

[47] N. Mangadoddy, Ram Prakash, R.P. Chhabra, V. Eswaran, Forced convection in cross flow of power law fluids over a tube bank, Chem. Eng. Sci. 59 (2004) 2213–2222.
[48] R.B. Bird, W.E. Stewart, E.N. Lightfoot, Transport Phenomena, second ed., John Wiley & Sons Inc., New York, 2002.
[49] R.P. Bharti, R.P. Chhabra, V. Eswaran, A numerical study of the steady forced convection heat transfer from an unconfined circular cylinder, Heat Mass Transfer (2006) in press. 10.1007/s00231-006-0155-1.
[50] V. Eswaran, S. Prakash, A finite volume method for Navier–Stokes equations, Proceedings of 3rd Asian CFD Conference, Bangalore, India, vol. 1, 1998, pp. 127–136.
[51] T. Hayase, J.A.C. Humphrey, R. Greif, A consistently formulated QUICK scheme for fast and stable convergence using finite volume iterative calculation procedures, J. Comput. Phys. 98 (1992) 108–118.
[52] A. Sharma, V. Eswaran, A finite volume method, in: K. Muralidhar, T. Sundararajan (Eds.), Computational Fluid Flow and Heat Transfer, Narosa Publishing House, New Delhi, 2003, pp. 445–482.
[53] A. Sharma, V. Eswaran, Effect of channel-confinement and aiding/opposing buoyancy on the two-dimensional laminar flow and heat transfer across a square cylinder, Int. J. Heat Mass Transfer 48 (2005) 5310–5322.
[54] J. Comiti, A. Montillet, D. Seguin, M. Hilal, Modelling of power-law liquid-solid mass transfer in packed beds in Darcy regime, Chem. Eng. J. 89 (2002) 29–36.
[55] G. Peev, A. Nikolova, D. Todorova, Mass transfer from solid particles to power-law non-Newtonian fluid in granular bed at low Reynolds numbers, Chem. Eng. J. 88 (2002) 119–225.
[56] R. Shukla, S.D. Dhole, R.P. Chhabra, V. Eswaran, Convective heat transfer for power law liquids in packed and fluidised beds of spheres, Chem. Eng. Sci. 59 (2004) 645–659.
[57] B.K. Rao, B.J. Phillips, J. Andrews, Heat transfer to viscoelastic polymer solutions flowing over a smooth cylinder, Appl. Mech. Eng. 1 (1996) 355–365.
[58] P.D.M. Spelt, T. Selerland, C.J. Lawrence, P.D. Lee, Flow of elastic non-Newtonian fluids through arrays of aligned cylinders, Part 1. Creeping flows, J. Eng. Math. 51 (2005) 57–80.